Continuous-wave cavity ringdown spectroscopy of the 8ν polyad of water in the $25\,195-25\,340\ \mathrm{cm}^{-1}$ range

Patrick Dupré, Titus Gherman, Nikolai F. Zobov, Roman N. Tolchenov, and Jonathan Tennyson

Citation: The Journal of Chemical Physics **123**, 154307 (2005);
View online: https://doi.org/10.1063/1.2055247
View Table of Contents: http://aip.scitation.org/toc/jcp/123/15
Published by the American Institute of Physics

Continuous-wave cavity ringdown spectroscopy of the 8ν polyad of water in the 25 195–25 340 cm^{-1} range

Patrick Dupré[a] and Titus Gherman[b]
Laboratoire de Spectrométrie Physique [associated with Centre National de la Recherche Scientifique (CNRS) Unite Mixte de Recherche (UMR) C5588], Université Joseph Fourier de Grenoble, BP 87 38402 Saint-Martin d'Hères Cedex, France

Nikolai F. Zobov,[c] Roman N. Tolchenov, and Jonathan Tennyson
Department of Physics and Astronomy, University College London, London WCIE 6BT, United Kingdom

(Received 28 March 2005; accepted 16 August 2005; published online 19 October 2005; publisher error corrected 1 December 2005)

State-of-the-art experiments and calculations are used to record and assign the data obtained in the weakly absorbing blue energy region of the H_2O spectrum. Continuous-wave cavity ringdown absorption spectroscopy with Doppler resolution is used to probe the range from 25 195 to 25 470 cm^{-1} with an absorption sensitivity of ~1 parts per 10^9 (ppb)/cm. 62 lines of the polyad $\nu_{OH}=8$ are reported, of which 43 are assigned using variational nuclear calculations. The study includes absorption line intensities (in the range of 10^{-28}–10^{-26} cm/molecule) for all lines and self-broadening pressure coefficient for a few lines. The newly obtained energy levels are also reported. © *2005 American Institute of Physics*. [DOI: 10.1063/1.2055247]

I. INTRODUCTION

Water is of predominant importance for terrestrial life and its spectrum has therefore been subject of numerous studies, both experimental and theoretical. It is a key molecule in the earth's climate system and its spectrum is now determined over a large frequency range. However, since water vapor is both the most abundant greenhouse gas and the major absorber of incoming sunlight, the precise determination of its absorption properties is crucial. In determining the energy balance between solar irradiance and the earth's infrared emission absorbed by the atmosphere, missing absorption lines in atmospheric models may cause serious discrepancies with the observed data.[1] Although this statement has been contradicted,[2] there is still a clear need for studies of weak water vapor transitions. The maximum solar emission is in the blue part of the spectrum which makes the absorption by water vapor in this wavelength region a key issue. The complexity of atmospheric models, which include huge quantities of data from laboratories, requires reliable data bases. Improving the quality of these bases [such as HITRAN (Ref. 3)] is a major aim of this paper.

Fourier transform spectroscopy (FTS) has been the traditional experimental source of water data. It is well known that the rotation-vibration spectrum of water, with its characteristics polyad structure[4–8] extends across the entire visible region. However, laser-based techniques can now successfully compete with FTS instruments as the challenge of observing weak transitions resides in long absorption equivalent path lengths or multipass absorption cell. Among laser techniques, the cavity ringdown spectroscopy (CRDS) offers several advantages and its potential is mainly limited by the quality of the mirrors constituting the optical cavity. Moreover, line intensity can be determined without any additional calibration procedure. The use of a continuous-wave (CW) source allows to investigate the line profiles even at a moderate pressure (~10 Torr). For example, our study shows that the water vapor line profiles exhibit a great variation in pressure dependence as a function of the studied transition. Water transitions as weak as 10^{-29} cm/mol have been observed in the near IR region of the spectrum (1.48–1.63 μm) by CW-CRDS (equivalent absorption length: ~27 km).[9] Note that an equivalent absorption length of ~120 km has been obtained by intracavity laser absorption spectroscopy (ICLAS) around 9600 cm^{-1}.[10]

The simplicity and sensitivity of the CRDS technique were demonstrated using water vapor, for example, around 1.1 μm, by Ramponi and co-authors who obtained a sensitivity of 5×10^{-8}/cm,[11] and around 833 nm by Zare's group who demonstrated a sensitivity of 1.7×10^{-9}/cm using heterodyne detection.[12,13] The pulsed-CRDS technique has been used by two groups for water spectroscopy purposes at ~810 nm in flame environment,[14] and in the 555-606 nm range in bulk cell.[15,16] In conjunction with a slit supersonic jet expansion, Saykally's group observed the multiple water clusters in the IR domain.[17–21]

The present work extends the previous FTS studies which reported seven lines ($S_0>0.46^{-26}$ cm/mol.) in the near ultraviolet.[22–25] It provides complementary data to the double photon excitation, quantum beat detection of photofragment laser-induced fluorescence spectrum[26] which

[a]Author to whom correspondence should be addressed. Present address: Laser Spectroscopy Facility, Department of Chemistry, The Ohio State University, Columbus, Ohio 43210. Electronic mail: pdupre@chemistry.ohio-state.edu
[b]Present address: Laboratoire de Génie Electrique de Toulouse, Université Paul Sabatier 118 Route de Narbonne, 31062 Toulouse Cedex, France.
[c]Permanent address: Institute of Applied Physics, Russian Academy of Science, Uljanov Street 46, Nizhnii Novgorod, Russia 603950.

probed the $J=1$ and 2 levels of the 8ν polyad. That study provided the value of the dipole moment of the various excited states using Stark effect.[27]

Assignment of the quantum numbers to the lines in the frequency range studied here represents quite a challenge. The relatively small range of frequencies probed means that, in the majority of cases, it was not possible to confirm the assignments of new energy levels by using combination differences. This means that the only practical approach for assigning the spectrum is by direct comparison with variational calculations. A new line list based on a previously published potential[28] is employed for this purpose. However, at the high frequencies probed here this analysis is by no means straightforward.

In this paper, Sec. II introduces the experimental setup, and Sec. III is devoted to the data analysis. Section IV presents the theoretical work, and compares the data and calculations. The results are discussed in the final section.

II. EXPERIMENT

The CRDS technique is an absorption-based spectroscopy tool which offers the major advantage of self-intensity calibration (it is insensitive to the source amplitude fluctuations); it does not require the knowledge of the source intensity, or of the sensitivity of the detector. However, a linear response of the medium under study is required to readily obtain the quantitative information.[29] Several review papers[30–37] have been devoted to this technique and only the relevant aspects will be presented here.

If optical cavities are ideal to reach long equivalent absorption pass, the cavity enhanced absorption spectroscopy (CEAS) technique and the CRDS technique could be considered as the equivalent techniques, however, at the opposite of the CRDS technique which is based on a time decay measurement, the CEAS technique suffers from the disadvantage of the sensitivity to the source amplitude fluctuations. On the other hand, when it is coupled to a broadband source, it can be a multiplex technique whose spectral resolution is limited by the dispersive device.[38–46]

The CRDS technique is based on the measurement of the additional losses induced inside a high-quality optical cavity (in other words, a Fabry–Perot filter) by the absorption of the medium under investigation. Because the quality coefficient of such a cavity can be very high ($Q \approx 2\times 10^{11}$), the photon trapping time [i.e., relaxation, characteristic,[47] or ringdown (RD) time τ_{RD}] inside the cavity may reach several hundreds of microseconds even for relatively short cavities.[48–52] Thus, the equivalent absorption length can reach several hundreds of kilometers, which is unreachable with multipass laboratory cells. Moreover, when the cavity is fully occupied by the absorber, the CRDS technique yields access directly to the Beer–Lambert law coefficient of absorption (α), and not to the absorbance itself (αl) as most other absorption techniques do.

The formal description of the time response of a cavity is straightforward, even if it has been the object of some controversy.[53] However, the exact time response of a cavity to a given source is not necessarily well understood in the presence of an absorber because of the difficulties of modeling the spatial coupling of the incoming beam with the cavity eigenmodes. For example, if the absorber susceptibility is not linear, or if the spectral linewidth of the source and of the absorber cannot be neglected, additional complications arise.[54] Reference 29 provides the required Fourier transform-based formalism for any kind of laser sources (if that can be modeled). Based on a pure energetic argument (no interference), it is easy to establish the time behavior of the electromagnetic (EM) field trapped inside a cavity; exponential decay (characterized by the RD time) of the EM since the cavity losses linearly depend upon the intensity of energy trapped. Assuming an ideal uniform linear absorption (in the angular frequency domain),

$$\frac{1}{\tau_{\mathrm{RD}}(\omega)} = \frac{1}{\tau_e} + c\alpha_0(\omega), \tag{1}$$

where c is the light speed, $\alpha_0(\omega)$ is the linear absorption, τ_e is the RD time of the empty cavity (weakly depending on ω), and diffraction losses are neglected.

There are some experimental difficulties in observing such a behavior which can only be achieved with good control on the cavity alignment and on the beam/cavity coupling. Assuming that an optimum alignment of the optical cavity is reached, then the beam injection needs to be controlled. For example, with spectrally broad sources (pulsed sources), (i) the incoming EM may not experience the same characteristics time for all of its Fourier components when interacting with the cavity modes [superimposition of eigentransverse cavity modes, i.e., transverse electromagnetic mode$(\mathrm{TEM})_{ij}$]; and (ii) the interferences between the different transverse and/or longitudinal modes can result in beating. Under such conditions, the global behavior will be a nonexponential decay which exhibits beating, bi- or multiexponential decays. To offset these problems, a concept of modeless or multimode cavity has been introduced.[55–60]

One way to approach the ideal response of the cavity [exponential decay following Eq. (1)] is to use a CW source whose spatial and spectral "purities" are usually significantly higher than any nanosecond-pulsed source can provide. This kind of source gives a good control of the coupling of the incoming beam to a TEM_{00} cavity mode, and of rejection of the higher-order transverse modes. Exponential decays over four decades may be observed,[29] and may even reveal some nonlinear response of the acquisition device chain. Under such conditions, the sensitivity of the technique is limited by the precision of the measurement of the RD time, $\Delta\tau_{\mathrm{RD}}/\tau_{\mathrm{RD}}$ [from Eq. (1)],

$$\frac{\Delta\alpha_0(\omega)}{\alpha_0(\omega)} = -2\frac{\Delta\tau_{\mathrm{RD}}(\omega)}{\tau_{\mathrm{RD}}(\omega)}. \tag{2}$$

It can be demonstrated that the minimum of sensitivity (per decay) is given by

$$\alpha_{0_{\min}} = \frac{1}{c\tau_e}\frac{\Delta\tau_{\mathrm{RD}}}{\tau_{\mathrm{RD}}} = \frac{1}{l_{\mathrm{eq}}}\frac{\Delta\tau_{\mathrm{RD}}}{\tau_{\mathrm{RD}}}. \tag{3}$$

Ideally, a laser source can be characterized by its spectral bandwidth, or by its coherence time assuming that the source

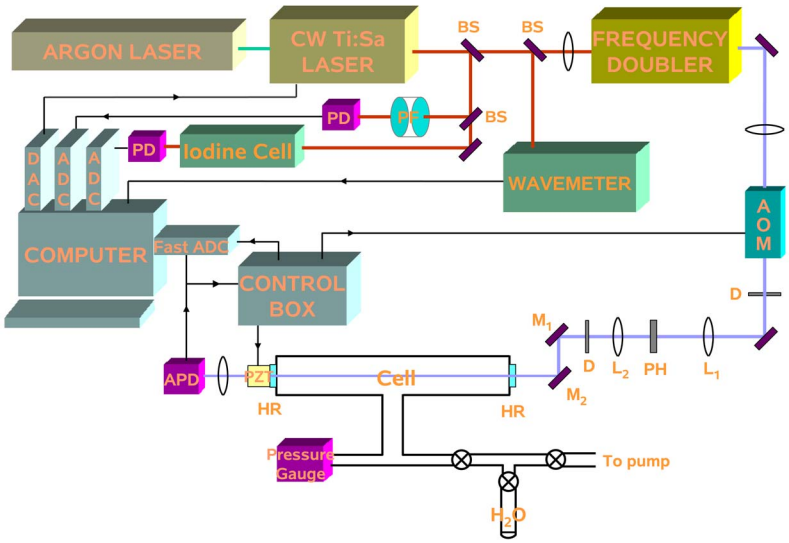

FIG. 1. Schematic diagram of the experimental setup. The abbreviations are as follows: beamsplitter (BS), Fabry–Perot etalon (FP), photodetector (PD), avalanche PD (APD), pinhole (PH), diaphragm (D), acousto optic modulator (AOM), cylindrical piezoelectric actuator (PZT), (micro translatable) lenses of the spatial filter L_1 and L_2 spatial filter lens (micro translatable), High reflector mirror (HR), M_1 and M_2 constitute a periscope.

is Fourier transform limited. The use of a single mode CW source (laser or diode) exhibiting a narrow bandwidth ($\Delta\nu_{\mathrm{las}} \sim 1$ MHz) prevents the simultaneous excitation of several longitudinal modes since the free spectral range (FSR) of any usual cavity is a lot larger than $\Delta\nu_{\mathrm{las}}$.

The observation of pure exponential decays using a CW source has a price in terms of complexity. It requires the matching of the laser source mode to one cavity mode, and an efficient optical switch to quickly interrupt the incoming EM field, and start the time decay acquisition. Less sophisticated setups have been proposed to avoid such a complexity,[61–71] for example, by periodically sweeping the source frequency through a cavity mode allowing the sweeping to act as a switch. Such setups do not allow for the control of the EM field intensity injected inside the cavity, and the interference of the frequency swept source beam with the cavity eigenmode leads to chirp beating.[68,72,73] Because the matching of the source and cavity modes is crucial, several kinds of servo loop have been proposed.[74–79] Furthermore, heterodyne detections have been recently proposed,[12,13,80–85] and these methods have demonstrated the best sensitivities, which are close to the shot noise.

The setup used for the water data acquisition is displayed in Fig. 1. The laser chain is based on a scannable, externally stabilized Ti:sapphire laser source (Coherent, model 899-21) delivering up to 2.5 W in a single mode (stability: ~0.5 MHz rms) when it is pumped (~15 W) by an Ar^+ laser source (Spectra Physics, model 2045). By using beam splitters (uncoated BK7 plates) small fractions (~1%) of the outgoing laser beam are directed to (i) a Fabry–Perot etalon (Eksma, finesse ~20) associated with a photodiode for linearization purpose, (ii) a 1-m-long iodine quartz cell (thanks to the University of Göttingen) warmed up to a temperature of 450 °C (and including a cold finger at a lower temperature) for calibration purposes, and (iii) a homemade (interferometer) lambdameter[86] for preselection of the wavelengths of interest. Frequencies in the blue are obtained by an external intracavity frequency doubling unit using a LBO crystal (Wavetrain, Laser Analytical System) generating up to 350 mW (Hänsch-Couillaud servo control).

The high finesse cavity is constituted by a cell supporting two high reflectance ($\mathcal{R} \sim 0.999\,973$) superpolished planoconcave mirrors (ROC ~ 1 m) from Research Electro Optics 0.35 m apart. The output mirror sits on a cylindrical piezoelectric actuator or PZT (PI) which allows the control of the cavity length. The incoming laser beam is "cleaned" by a spatial filter (lens L_1, pinhole PH, lens L_2, and diaphragm D). The central lobe of the diffraction figure is close to the Gaussian shape of a pure TEM_{00} transverse mode. The adjustable position of lens L_2 complemented by the periscope (mirrors M_1 and M_2) provides a good overlap between the laser beam and a TEM_{00} mode of the cavity; rejection of the higher-order modes of 100:1 has be routinely observed inside an evacuated chamber. The beam size at the center of the cavity [waist half-width at half maximum (HWHM)] has been estimated at 260 μm, at the mirrors, the beam size increase is limited to ~10%. This excludes any significant diffraction losses due to the limited size of the mirrors (diameter: ~7.75 mm). The beam transmitted through the cavity is collected on a thermally controlled fast silicon avalanche photodiode (APD) (Hamamatsu model S6045-04) feeding a homemade large bandwidth transimpedance amplifier ($R_F = 50\ \mathrm{k}\Omega$).

The APD detector is used for two purposes: to servocontrol the cavity length and to acquire the RD time. This is possible by setting two different voltage thresholds (the acquisition can only happen after an efficient tracking of the cavity length for a maximum of transmission). The control of the cavity length stems from a homemade control box based on a modulation (100–500 Hz) of the cavity length whose amplitude induces a modulation of a few percent of the cavity bandwidth.[29,74] Due to the finesse of the cavity (~140 000), the bandwidth of the longitudinal mode is very narrow (~3.1 kHz HWHM) compared to the short time-averaged laser spectral linewidth (~0.5 MHz). The required mode matching is obtained by slightly modulating the high voltage applied to the PZT crystal actuator through a servo controlled dc high voltage obtained by the amplitude symmetrization of the modulation around a maximum of transmission. This "crude" control does not allow a continu-

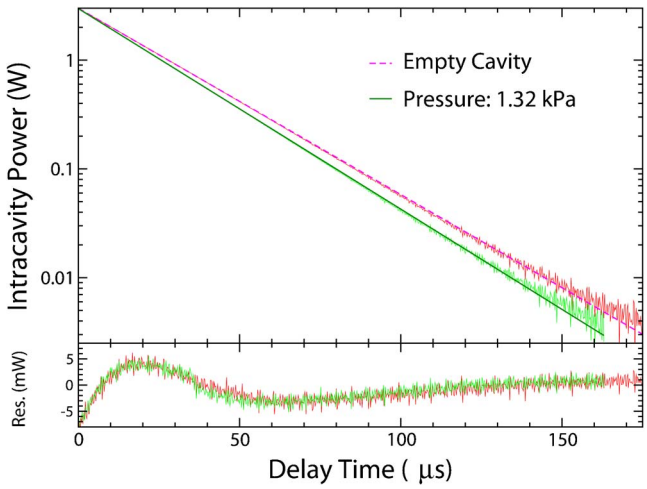

FIG. 2. Example of decays which shows the time evolution for (i) the empty cavity and (ii) the cavity filled by 1.32 kPa (9.9 Torr) of water at room temperature. The laser source was fixed at the center of the transition $4_{31} \leftarrow 3_{12}$, $(8,0)^{-}0$ (25 259.3524 cm^{-1}). τ_e=25.36(8) μs, τ_0=23.56(8) μs, with 1024 averages. Intracavity power was estimated from the transmission of the mirrors and from the the responsivity of the detector.

ous injection of the EM field inside the cavity (since the modulation is larger than the laser bandwidth and, of course, of the cavity mode bandwidth), however, it does provide the required tracking of the cavity, even when the laser is frequency scanned. When a mode matches the incoming EM field, the intensity of the trapped EM field increases (buildup) until it reaches a predetermined threshold which delivers a trigger signal for (i) first switching off the laser beam through the acousto-optic modulator (AOM) (from AA Opto-Electronique) and its driver, (ii) then triggering the RD decay acquisition, and (iii) stopping the cavity modulation during the acquisition time. The AOM is activated by a rf signal at 110 MHz and diffracts in the −1 order (the zero diffraction order is blocked). The switching time is estimated to be less than 200 ns, and the rejection rate is higher than 70 dB (Mini-Circuits device). The threshold intensity for the RD acquisition is estimated ~3 W.

The entire setup is driven by a personal computer, the interface software was built with LABVIEW (National Instruments) including "*c*" optimized additional routines. The RD signal is acquired on a 5 MHz, 12-bit data acquisition card (National Instruments) connected on the PCI bus. The RD decays can be accumulated before analysis, and then possibly averaged. At each scan step, the RD time is determined from the acquired data after correction of the nonlinearities of the analog-to-digital converter (ADC), and by running a linear regression on the (pretabulated) logarithm of the offset freed data. This regression is carefully weighted to take into account a constant technical noise (1-2 mV), since the intensity of the collected signal (a few tens of microwatts) provides a negligible photon noise in comparison to all other noise sources. In addition, the algorithm has the capability of self-rejecting a decay, which would have an unexpected decay time, usually when a non-TEM_{00} mode is excited (such a mode exhibit a shorter decay time). A typical averaged decay is given in Fig. 2 for both evacuated and under usual H_2O pressure condition cavity. The linearity of the absorption of the water lines versus the intensity of the trapped EM field has been checked inside the energy region under study and up to an EM field of 5 W. This check shows that the value of the acquisition trigger threshold is not important, however, after we have determined the mirror transmission and the responsivity of the detector, a linear relation has been established between the recorded voltage, and the intensity of the trapped intracavity EM field.

The decays are very close to a pure exponential shape over more than three orders of magnitude. However, a great number of averaged decays reveal small distortions due to residual unidentified nonlinearities showing residual oscillations of about 0.1%. These oscillations can be eliminated by fitting with a triexponential decay (not shown on the pictures and not performed in our analysis), the residual signal then exhibits a quasi-Gaussian noise intensity whose relative standard error is $\sim 0.25 \times 10^{-3}$. Finally, we note that the decays, obtained at the end of a running day, exhibit a slightly shorter RD time because the slight surface adsorption of the water vapor on the mirrors, slightly reducing the finesse of the cavity.

The scan of the Ti:Sa laser is externally controlled by the PC through a 16-bit digital-to-analog converter (DAC). Each scan is usually on the order of 2.2 cm^{-1} (after frequency doubling) with 8196 step points. The effective average acquisition rate is on the order of 50 Hz (Pentium II at 333 MHz), and is mainly limited by the data transfer rate on the PCI bus and by the fitting process. The resulting rms normalized sensitivity is $\sim 5.7 \times 10^{-9}$ $cm^{-1}/\sqrt{Hz}$.

In this setup, the main problem stems from the relatively poor stability of the water pressure (~10 Torr) inside the chamber monitored by a Baratron gauge whose actual values were used in the data analysis.

III. DATA ANALYSIS

The linear corrections required by the scan are obtained by determining, after smoothing (usually 16 points), the maxima of the transmission of the 5-cm-long Fabry–Perot solid etalon, and by fitting these maxima to a fifth-order polynomial. Reference iodine lines are used for calibration purposes. The experimental iodine line centers are determined by fitting a Gaussian profile and used as inputs with a Newton polynomial shape. The reference line positions are obtained, either from the line centers published in the I_2 atlas,[87] or by fitting a Gaussian line profile calculated from IODINESPEC[88] by including the hyperfine structure and assuming a temperature of 500 K. The different scans overlap each other so that at least 2 calibration lines can be used for all of them. After a complete calibration of the stepwise spectrum, the steps are put side to side by averaging the multiscanned areas. The offset frequency, introduced by the AOM, is also removed from the data.

An absorption spectrum results from the conversion of the data based on formula (1). For each line, the absorption cross section is deduced by calculating the line integral (obtained by fitting) and from the pressure measured during the scans. When the signal-to-noise ratio is large enough, a Voigt profile is used by constraining the Doppler contribution (γ_D)

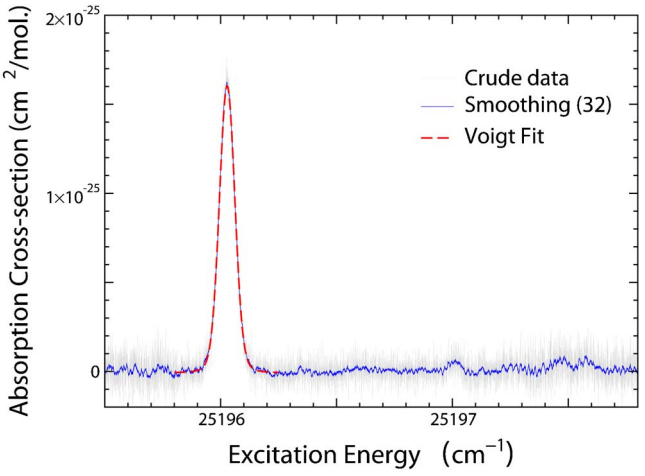

FIG. 3. Part of the CW-CRDS spectrum which mainly shows the transition $(8,0)^+0$, $4_{23} \leftarrow 3_{12}$ at a pressure of ~10 Torr (~1.3 kPa). For visual inspection purposes, the crude data has been smoothed. Using a Voigt profile fit (assuming γ_D=0.0368 cm^{-1} HWHM), the following information was deduced: σ_0=25 196.0280(20) cm^{-1}, S_0=1.45(12)10^{-26} cm/mol, and γ_{col} =0.0043(12) cm^{-1} (HWHM).

to the value determined by the temperature of the experiment, see, for example, Fig. 3. In other cases, a simple Doppler profile is assumed. Two algorithms are used, either MULTILINE[89] based on the "ROOT" package (root.cern.ch), or a package developed by one of the authors.[90] Figure 3 shows a minimum detectivity of the cross section of ~5 $\times 10^{-27}$ cm^2/mol. In this analysis the possibility of more complex line profiles is excluded.

To calibrate the data given in Table I, an absolute intensity is obtained from the strongest line $4_{23} \leftarrow 3_{12}$, $(8,0)^+0$ at 25 196.028 cm^{-1}, see Fig. 3, of 1.41×10^{-26} cm/mol in excellent agreement with the FTS value of Coheur *et al.*[24] The absolute intensity of the other line is determined as a ratio from this value. This procedure was checked by refitting three other lines to obtain direct intensities and found to reproduce the result within 10%. Overall, our intensities are accurate to better than 20%, except for the weakest lines where a larger error is to be expected.

IV. CALCULATIONS: LINE ASSIGNMENT AND INTENSITY

Despite recent significant advances in the *ab initio* calculation of water rotation-vibration spectra,[91] such calculations are not accurate enough to match the spectra at the high excitation energies probed here. Similarly, line lists based on spectroscopically determined potentials do not necessarily perform well at these frequencies. For example, Partridge-Schwenke line list,[4] which has been widely used to analyze spectra at near-infrared and visible wavelengths, is of no help at these frequencies. This is unsurprising as it is well established that the calculations based on spectroscopically determined potentials do not extrapolate reliably to regions for which there was no data in the original fit.[92] Recently, Shirin *et al.*[93] have obtained a new spectroscopically determined potential for $H_2^{16}O$. This potential was constructed by starting from high-quality *ab initio* electronic structure calculations augmented by explicit inclusion of corrections due to electronic relativistic effect, the Lamb shift, and the inclusion of both adiabatic and nonadiabatic non-Born-Oppenheimer corrections. Spectroscopic data covering the entire range of observed water spectra was used to refine the potential which was found, particularly, to give significantly more reliable results for the higher frequencies used than the previous studies. We use an extended version of the variational line list based upon this potential which was computed previously for transition with visible frequencies.[28]

The intensities were calculated using the carefully fit dipole moment surface of Schwenke and Partridge.[94] As can be seen from Table I, the calculated and measured intensities are generally in good agreement.

Making assignments without the aid of combination differences is difficult and often unreliable. However, there are aspects which aided the procedure in this case. First there are fewer strong lines in this frequency range than at lower frequencies. Second, as can be seen from Fig. 4 and Tables II and III, there is a systematic shift between our predicted line positions and observations.

The good agreement between the predicted and observed intensities of the individual lines is a tribute to the dipole moment surface of Schwenke and Partridge which is far superior to other available water dipole surfaces for this region. In fact the Stark-induced quantum beat experiments of Callegari *et al.*[27] provides an extremely stringent test of the calculated dipoles. These experiments show that, at least for highly excited states, the variational calculations are able to reproduce the observed dipole moments to within a few percent.

There is one further difficulty with interpreting the spectra which concerns the use of approximate quantum numbers. Variational calculations only use rigorous quantum numbers which, in the case of H_2O, correspond to the rotational angular momentum N, the parity p, and the ortho/para symmetry. The standard vibrational labels, in either normal-mode or local mode form and the asymmetric top quantum numbers K_a and K_c are only approximate. There are several schemes for matching the calculated states and approximate quantum numbers for highly excited states of water.[4,95,96] Previous assignments in the present region have only involved transitions to the $(8,0)^{\pm}0$ states. Assigning vibrational labels to the further transitions involving these states was straightforward but left us with a number of candidate transitions to the previously unobserved vibrational states. Vibrational labels for these states could be approximately determined using a procedure based on analysis of energy levels[95] and confirmed by plotting the vibrational wave functions. In practice, no more than a single transition to any vibrational state other than the $(8,0)^{\pm}0$ states could be made, so it was not possible to assign transitions to other vibrational states with any confidence.

V. DISCUSSION

The line-by-line analysis of the spectrum from 25 195 to 25 395 cm^{-1} is presented in Table I and Fig. 4. Only the lines with an intensity higher than the noise level, usually about 2×10^{-28} cm^{-1}, are reported with the additional constraint

TABLE I. Analysis of the H_2O spectrum between 25 195 and 25 337 cm^{-1} at 300 K, lower vibrational state: (0, 0, 0). The uncertainties are expressed in the unit of the last digit. When there are no additional indication, the rotational and vibrational assignments refer to the same authors.

Line center (cm^{-1})		S_0(10^{-26} cm/mol.)		Pressure self-broadening[a] (10^{-6} cm^{-1}/Pa)	$N'_{K'_aK'_c}$	$N''_{K''_aK''_c}$	Band
Expt.	Calc.	Expt.	Calc.				
25 196.0281 (20)	25 195.61	1.45 (12)[b]	1.71	3.2 (9)	$4_{2\,3}$	$3_{1\,2}$	$(8,0)^+0$
25 196.0385[c]					$4_{2\,3}$	$3_{1\,2}$	$(8,0)^+0$
25 196.0363 (53)[d]		1.42 (25)		NA	$4_{2\,3}$	$3_{1\,2}$	$(8,0)^+0$
25 196.024					NA	NA	NA
25 197.0075 (35)	25 197.09	0.034 (14)	0.04	NA	$7_{7\,0}$	$6_{6\,1}$	$(8,0)^+0$
25 197.4670 (35)	25 198.05	0.061 (25)	0.10	NA	$7_{3\,5}$	$6_{2\,4}$	$(8,0)^+0$
25 197.5656 (35)		0.056 (24)		NA			
25 205.7407 (18)	25 205.29	0.19 (4)	0.23	4.4 (2.2)	$2_{2\,0}$	$1_{0\,1}$	$(8,0)^-0$
25 206.3465 (60)	25 260.81	0.05 (2)	0.06	NA	$8_{4\,5}$	$7_{3\,4}$	$(8,0)^+0$
25 212.0531 (16)	25 211.76	0.95 (9)	0.58	19 (6)	$6_{3\,4}$	$5_{2\,3}$	$(8,0)^+0$
	25 211.63		0.38		$3_{3\,1}$	$2_{2\,0}$	$(8,0)^+0$
25 212.050[c]					$3_{3\,1}$	$2_{2\,0}$	$(8,0)^+0$
25 212.0440 (56)[d]		1.53 (34)		18.7 (9.7)	$3_{3\,1}$	$2_{2\,0}$	$(8,0)^+0$
25 213.5068 (16)	25 213.12	1.01 (9)	1.07	3.7 (1.1)	$3_{3\,0}$	$2_{2\,1}$	$(8,0)^+0$
25 313.5265 (55)[d]		1.54 (36)		9.3 (7.5)	NA	NA	NA
25 313.498[e]					NA	NA	NA
25 215.3880 (16)	25 214.95	0.46 (5)	0.50	2.2 (9)	$3_{2\,1}$	$2_{1\,2}$	$(8,0)^+0$
25 215.3992 (57)[d]		0.58 (24)		NA	NA	NA	NA
25 215.8825 (18)	25 215.86	0.28 (5)	0.14	13 (7)	$6_{6\,1}$	$5_{5\,0}$	$(8,0)^+0$
	25 215.84		0.05		$6_{6\,0}$	$5_{5\,1}$	$(8,0)^+0$
25 216.9321 (30)		0.076 (20)		NA			
25 218.4079 (30)		0.080 (20)		NA			
25 219.0878 (15)	25 218.71	1.40 (12)	1.10	11 (3)	$4_{3\,2}$	$3_{2\,1}$	$(8,0)^+0$
	25 218.78		0.29		$5_{3\,3}$	$4_{2\,2}$	$(8,0)^+0$
25 219.0955[c]					$4_{3\,2}$	$3_{2\,1}$	$(8,0)^+0$
25 219.0926 (54)[d]		1.73 (31)		6.2 (5.2)	$4_{3\,2}$	$3_{2\,1}$	$(8,0)^+0$
25219.072[e]					NA	NA	NA
25 221.4198 (60)		0.07 (3)		NA			
25 222.1052 (60)		0.07 (3)		NA			
25 222.2001 (55)		0.11 (5)		NA			
25 224.4880 (60)		0.09 (4)		NA			
25 224.8736 (50)	25 224.58	0.99 (9)	0.81	11 (3)	$4_{4\,1}$	$3_{3\,0}$	$(8,0)^+0$
	25 224.36		0.16		$3_{2\,1}$	$2_{0\,2}$	$(8,0)^-0$
25 224.8963[c]					$4_{4\,1}$	$3_{3\,0}$	$(8,0)^+0$
25 224.9093 (62)[d]		0.43 (32)		NA	$4_{4\,1}$	$3_{3\,0}$	$(8,0)^+0$
25 225.1095 (50)	25 224.81	0.29 (6)	0.26	6 (4)	$4_{4\,0}$	$3_{3\,1}$	$(8,0)^+0$
25 226.2031 (50)	25 226.05	0.41 (7)	0.27	4 (3)	$4_{3\,1}$	$3_{2\,2}$	$(8,0)^+0$

TABLE I. (*Continued.*)

Line center (cm^{-1})		S_0(10^{-26} cm/mol.)		Pressure self-broadening[a] (10^{-6} cm^{-1}/Pa)	$N'_{K'_aK'_c}$	$N''_{K''_aK''_c}$	Band
Expt.	Calc.	Expt.	Calc.				
25 226.4146 (50)	25 226.13	0.30 (6)	0.30	9 (5)	$5_{5\,0}$	$4_{4\,1}$	$(8,0)^+0$
25 226.5280 (60)	25 226.11	0.09 (4)	0.10	NA	$5_{5\,1}$	$4_{4\,0}$	$(8,0)^+0$
25 227.4455 (50)	25 227.33	0.17 (5)	0.23	NA	$6_{5\,2}$	$5_{4\,1}$	$(8,0)^+0$
25 228.3494 (60)		0.08 (5)		NA			
25 229.2490 (60)		0.07 (4)		NA			
25 229.4544 (60)		0.09 (5)		NA			
25 229.9079 (55)		0.09 (3)		NA			
25 230.3729 (50)	25 230.10	0.16 (5)	0.20	2.0 (1.4)	$5_{4\,2}$	$4_{3\,1}$	$(8,0)^+0$
25 230.7014 (50)	25 230.70	0.26 (6)	0.23	2.5 (1.5)	$6_{4\,3}$	$5_{3\,2}$	$(8,0)^+0$
25 231.2254 (60)		0.07 (3)		NA			
25 231.4148 (50)		0.13 (4)		NA			
25 231.9886 (50)	25 231.71	0.46 (8)	0.56	NA	$5_{4\,1}$	$4_{3\,2}$	$(8,0)^+0$
25 232.0041(58)[d]		0.63(31)		NA	NA	NA	NA
25 231.999[e]					NA	NA	NA
25 232.3158 (60)		0.09 (4)		NA			
25 233.0893 (60)		0.08 (4)		NA			
25 236.7819 (60)	25 236.61	0.12 (5)	0.09	NA	$6_{4\,2}$	$5_{3\,3}$	$(8,0)^+0$
25 237.8884 (60)		0.06 (3)		NA			
25 238.1514 (60)		0.07 (4)		NA			
25 239.8446 (50)	25 239.49	0.48 (8)	0.38	NA	$5_{3\,2}$	$4_{2\,3}$	$(8,0)^+0$
25 241.0863 (60)		0.03 (2)		NA			
25 241.6670 (60)	25 241.26	0.06 (3)	0.06	NA	$4_{2\,2}$	$3_{1\,3}$	$(8,0)^+0$
25 247.1905 (50)	25 246.78	0.35 (7)	0.49	NA	$4_{2\,2}$	$3_{0\,3}$	$(8,0)^-0$
25 259.3524 (50)	25 258.98	0.42 (7)	0.43	NA	$4_{3\,1}$	$3_{1\,2}$	$(8,0)^-0$
25 264.7105 (50)	25 264.36	0.17 (5)	0.17	7 (3)	$5_{3\,2}$	$4_{1\,3}$	$(8,0)^-0$
25 268.6938 (55)	25 268.30	0.11 (4)	0.14	NA	$3_{3\,1}$	$2_{1\,2}$	$(8,0)^-0$
25 272.4294 (50)	25 272.10	0.30 (7)	0.39	2.7 (1.5)	$6_{3\,3}$	$5_{1\,4}$	$(8,0)^-0$
25 273.8919 (60)	25 273.51	0.08 (4)	0.11	NA	$5_{2\,3}$	$4_{0\,4}$	$(8,0)^-0$
25 294.1111 (50)	25 293.91	0.17 (5)	0.26	NA	$6_{4\,2}$	$5_{2\,3}$	$(8,0)^-0$
25 298.1939 (50)	25 297.87	0.14 (5)	0.17	NA	$4_{4\,0}$	$3_{2\,1}$	$(8,0)^-0$

TABLE I. (*Continued.*)

Line center (cm^{-1})		$S_0(10^{-26}$ cm/mol.)		Pressure self-broadening[a] (10^{-6} cm^{-1}/Pa)	$N'_{K'_aK'_c}$	$N''_{K''_aK''_c}$	Band
Expt.	Calc.	Expt.	Calc.				
25 298.7198(60)	25 298.44	0.05 (3)	0.09	NA	$5_{4\,1}$	$4_{2\,2}$	$(8,0)^-0$
25 303.8590(55)	25 303.53	0.12 (4)	0.16	NA	$6_{2\,4}$	$5_{0\,5}$	$(8,0)^-0$
25 304.0127(60)	25 303.71	0.04 (2)	0.06	NA	$4_{4\,1}$	$3_{2\,2}$	$(8,0)^-0$
25 309.9988(50)	25 309.72	0.18 (5)	0.21	6 (3)	$5_{3\,3}$	$4_{1\,4}$	$(8,0)^-0$
25 313.8524(50)	25 313.58	0.17 (5)	0.24	NA	$5_{4\,2}$	$4_{2\,3}$	$(8,0)^-0$
25 328.7718(60)		0.02 (1)		NA			
25 329.4484(55)	25 329.28	0.11 (4)	0.11	NA	$6_{5\,1}$	$5_{3\,2}$	$(8,0)^-0$
25 329.8629(60)	25 329.70	0.025(12)	0.04	NA	$5_{5\,0}$	$4_{3\,1}$	$(8,0)^-0$
25 331.2073(60)	25 331.03	0.08 (3)	0.11	NA	$5_{5\,1}$	$4_{3\,2}$	$(8,0)^-0$
25 331.9473(60)	25 331.64	0.03 (2)	0.05	NA	$6_{3\,4}$	$5_{1\,5}$	$(8,0)^-0$
25 332.8719(60)	25 333.11	0.055(25)	0.08	NA	$7_{4\,4}$	$6_{2\,5}$	$(8,0)^-0$
25 334.1439(60)	25 334.05	0.03 (2)	0.05	NA	$6_{5\,2}$	$5_{3\,3}$	$(8,0)^-0$
25 335.0717(60)	25 335.19	0.07 (3)	0.08	NA	$7_{5\,3}$	$6_{3\,4}$	$(8,0)^+0$
25 336.5546(60)	25 336.53	0.025(12)	0.04	NA	$8_{6\,2}$	$7_{4\,3}$	$(8,0)^-0$

[a]Assuming a Voigt profile with a Doppler linewidth of 0.0368 cm^{-1} (HWHM), NA indicates that a Doppler profile was used (see text).
[b]Intensity used for reference.
[c]From Ref. 23.
[d]From Ref. 25.
[e]From Ref. 22.

for weak lines that their profile has to be compatible with a Doppler profile. If the lines are strong enough a pressure self-broadening coefficient was determined from the Lorentzian contribution to the profile (γ_{col}). Although the spectrum

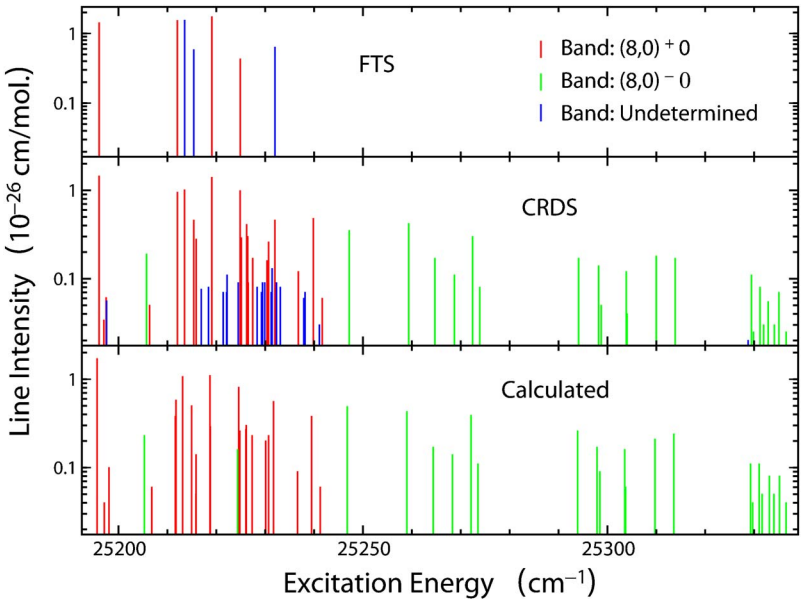

FIG. 4. Comparison of the simulated spectra between 25 195 and 25 337 cm^{-1} at 300 K (see Table I for more details). The spectrum is dominated by the *R* branch (i) of the band $(8,0)^+0$ ($\Delta K_a=2$) at low energy, and (ii) by the band $(8,0)^-0$ ($\Delta K_a=1$) at high energy.

TABLE II. Energy levels of the $(8,0)^+0$ or (800) vibrational state. Level energies for the ground state are available in Ref. 7. The uncertainties are expressed in the unit of the last digit.

$N_{K_aK_c}$	Level energy (cm^{-1})	Level[a]	Ref.	Obs.–Calc. (cm^{-1})
$1_{0\,1}$	25 140.597 (50)		[b]	0.50
$1_{1\,1}$	25 150.120 (50)		[b]	0.46
$1_{1\,0}$	25 154.610 (50)		[b]	0.46
$2_{0\,2}$	25 179.990 (50)		[b]	0.48
$2_{1\,2}$	25 180.0119 (22)	4	[c]	0.49
$2_{1\,1}$	25 199.780 (50)		[b]	0.48
$2_{2\,1}$	25 228.250 (50)		[b]	0.41
$2_{2\,0}$	25 229.510 (50)		[b]	0.43
$3_{0\,3}$	25 236.4598 (27)	3	[c]	0.45
$3_{1\,2}$	25 266.4814 (27)	3	[c]	0.46
$3_{2\,2}$	25 289.2417 (31)	2	[c]	0.45
$3_{2\,1}$	25 294.8844 (16)	1	[d]	0.43
$3_{3\,1}$	25 348.2312 (31)	2	[c,d]	0.43
$3_{3\,0}$	25 348.4084 (16)	1	[d]	0.38
$4_{1\,4}$	25 308.6551 (31)	2	[c]	0.46
$4_{2\,3}$	25 369.3955 (20)	5	[c,d]	0.42
$4_{2\,2}$	25 383.9337 (31)	2	[c,d]	0.38
$4_{3\,2}$	25 431.2457 (27)	3	[c,d]	0.38
$4_{3\,1}$	25 432.5045 (50)	1	[d]	0.15
$4_{4\,1}$	25 510.3149 (27)	3	[c,d]	0.32
$4_{4\,0}$	25 510.3288 (50)	1	[d]	0.30
$5_{0\,5}$	25 396.7352 (31)	2	[c]	0.42
$5_{1\,5}$	25 396.7455 (31)	2	[c]	0.43
$5_{1\,4}$	25 458.1293 (31)	2	[c]	0.41
$5_{2\,4}$	25 467.9783 (31)	2	[c]	0.36
$5_{3\,3}$	25 534.8673 (15)	1	[d]	0.32
$5_{3\,2}$	25 540.2069 (50)	1	[d]	0.35
$5_{4\,2}$	25 614.2154 (50)	1	[d]	0.28
$5_{4\,1}$	25 614.5055 (50)	1	[d]	0.28
$5_{5\,1}$	25 714.6622 (60)	1	[d]	0.43
$5_{5\,0}$	25 714.5223 (50)	1	[d]	0.29
$6_{0\,6}$	25 499.1201 (31)	2	[c]	0.16
$6_{1\,6}$	25 499.3807 (22)	4	[c]	0.38
$6_{1\,5}$	25 578.7382 (31)	2	[c]	0.26
$6_{3\,4}$	25 658.5638 (16)	1	[d]	0.29
$6_{4\,3}$	25 739.5135 (50)	1	[d]	0.01
$6_{4\,2}$	25 740.7500 (60)	1	[d]	0.17
$6_{5\,2}$	25 837.7867 (50)	1	[d]	0.13
$6_{6\,1}$	25 957.9589 (18)	1	[d]	0.03
$6_{6\,0}$	25 957.9556 (18)	1	[d]	0.05
$7_{0\,7}$	25 617.6268 (31)	2	[c]	0.44
$7_{1\,6}$	25 714.6131 (31)	2	[c]	0.45
$7_{3\,5}$	25 800.2405 (35)	1	[d]	−0.58
$7_{5\,3}$	25 984.0504 (60)	1	[d]	−0.11

[a]Number of levels used to characterize the level.
[b]From Ref. 97.
[c]From Ref. 7.
[d]This work.

TABLE III. Energy levels of the $(8,0)^-0$ or (701) vibrational state. Level energies for the ground state are available in Ref. 7.

$N_{K_aK_c}$	Level energy (cm^{-1})	Level[a]	Ref.	Obs.–Calc. (cm^{-1})
$0_{0\,0}$	25 120.2779 (31)	2	[b]	0.52
$1_{0\,1}$	25 140.6174 (40)	1	[b]	0.51
$1_{1\,1}$	25 150.1626 (22)	4	[b]	0.50
$1_{1\,0}$	25 154.6436 (31)	2	[b]	0.48
$2_{1\,1}$	25 199.7888 (18)	6	[b]	0.48
$2_{2\,1}$	25 228.3020 (31)	2	[b]	0.46
$2_{2\,0}$	25 229.5380 (20)	5	[b,c]	0.45
$3_{0\,3}$	25 236.4406 (31)	2	[b]	0.43
$3_{1\,3}$	25 239.8522 (31)	2	[b]	0.47
$3_{1\,2}$	25 266.5047 (31)	2	[b]	0.48
$3_{2\,2}$	25 289.2211 (23)	4	[b]	0.43
$3_{2\,1}$	25 294.9014 (26)	3	[b,c]	0.45
$3_{3\,1}$	25 348.1911 (35)	3	[b,c]	0.39
$3_{3\,0}$	25 348.3827 (31)	2	[b]	0.35
$4_{0\,4}$	25 310.1427 (20)	5	[b]	0.44
$4_{1\,3}$	25 353.2988 (27)	3	[b]	0.44
$4_{2\,2}$	25 383.9522 (50)	1	[c]	0.41
$4_{3\,1}$	25 432.7182 (50)	1	[c]	0.37
$4_{4\,1}$	25 510.6141 (60)	1	[c]	0.31
$4_{4\,0}$	25 510.3489 (27)	3	[b,c]	0.31
$5_{0\,5}$	25 396.1282 (60)[d]	1	[c]	0.44
$5_{1\,5}$	25 396.1282 (22)	4	[b]	0.44
$5_{1\,4}$	25 458.2018 (40)	1	[b]	0.50
$5_{2\,4}$	25 468.2278 (31)	2	[b]	0.63
$5_{2\,3}$	25 495.9446 (60)	1	[c]	0.38
$5_{3\,3}$	25 534.8372 (50)	1	[c]	0.28
$5_{3\,2}$	25 540.2075 (50)	1	[c]	0.35
$5_{4\,2}$	25 614.2147 (50)	1	[c]	0.27
$5_{4\,1}$	25 614.4993 (60)	1	[c]	0.27
$5_{5\,1}$	25 713.7242 (60)	1	[c]	0.18
$5_{5\,0}$	25 713.7054 (60)	1	[c]	0.16
$6_{2\,4}$	25 629.2069 (55)	1	[c]	0.34
$6_{3\,4}$	25 658.5727 (60)	1	[c]	0.32
$6_{3\,3}$	25 671.8869 (50)	1	[c]	0.32
$6_{4\,2}$	25 740.6217 (50)	1	[c]	0.21
$6_{5\,2}$	25 838.1120 (60)	1	[c]	0.10
$6_{5\,1}$	25 838.2605 (55)	1	[c]	0.18
$7_{4\,4}$	25 885.7833 (60)	1	[c]	-0.23
$8_{6\,2}$	26 267.7918 (60)	1	[c]	0.03

[a]Number of levels used to characterize the level.
[b]From Ref. 7.
[c]This work.
[d]Degenerescence assumed with the level $5_{1\,5}$.

was scanned from 25 195 to 25 470 cm^{-1} but some regions were not carefully analyzed because a visual inspection showed that no lines were observable; the existence of additional lines in the intensity range from 2×10^{-28} to 5×10^{-28} cm/mol cannot be entirely excluded.

The analysis of the experimental data using our new variational calculations allowed us to assign 37 new energy levels and 38 new transitions; 19 observed transitions stay unassigned. The assignment of the previously observed transitions are confirmed. Our data show an averaged difference between the observed and calculated transition energy of ~0.19 cm^{-1} slightly less than the standard error (~0.27 cm^{-1}) for the transition $(8,0)^+0$, and of ~0.25 cm^{-1} with a standard error of ~0.18 cm^{-1} for the transition $(8,0)^-0$. These differences are more than an order of magnitude larger than the experimental accuracy. The intensities of the calculated and observed lines are in good agreement since the relative difference is, on average, equal to 29% and always less than 80%. Some unassigned transitions are relatively strong; the strongest one is 0.13×10^{-26} cm/mol, their assignment will require a future work.

Our data and the recent FTS measurements[25] are in rea-

sonable agreement for the intensities and the pressure self-broadening coefficients. The only discrepancy concerns the line frequencies which show a small, systematic shift. Neglecting one pair of blended lines, which are therefore problematic, the remaining five lines common to both spectra are found at slightly lower wave numbers in our spectrum. The average shift is 0.0141 cm^{-1} with a standard deviation of only 0.0023 cm^{-1}. This shift is outside the calibration errors of both experiments. However the lines we are comparing are at the edge of the FTS spectrum and are also very weak in this spectrum, so it would seem more likely that this small error arises from that experiment. Furthermore we note that, for the few transitions available, our data give a better agreement with the measurements of Camy-Peyret *et al.*[22] than the more recent FTS measurements.[23]

The energy levels observed in both $(8,0)^+0$ and $(8,0)^-0$ bands with the same rotational quantum numbers are very close (<1 cm^{-1}), as is expected in strongly local mode states. However, the levels $5_{5\,0}$ and $5_{5\,1}$ do not follow this and are separated by about 2 cm^{-1} as they undergo a strong resonance interaction. Our calculations suggest that the perturbing state is a vibrational state (3,5,2) which has a calculated separation of about 1.7 cm^{-1}. The potential energy surfaces (PESs) needs to be improved further to accurately model this resonance interaction.

VI. CONCLUSIONS

A total of 62 near-ultraviolet water vapor transitions are observed, including 55 newly observed transitions. Assignment of the experimental data is based on new variational nuclear motion calculated using a spectroscopically determined potential-energy surface. 43 of these transitions are assigned, 4 as blends. All assigned transitions belong to the 8ν polyad, either to the $(8,0)^+0$ or the $(8,0)^-0$ stretching modes. They are all R branch transitions. Following our assignments, 43 energy levels of the band $(8,0)^+0$ are now determined, 17 for the first time, and 39 energy levels of the band $(8,0)^-0$ are determined, 19 for the first time. These energy levels are given in Table II.

The measurement of weak transitions is made possible because the intrinsic qualities of the CW-CRDS technique, mainly the absolute absorption determination and the long equivalent absorption length. However, this technique can be pushed further to gain another order of magnitude in the line intensity limit, mainly by decreasing the detection noise level.

The reported lines are weak but not necessarily insignificant for atmospheric purposes given the long pathlength of the sunlight through the earth's atmosphere and the higher energy carried by photons in the near UV than in regions where water absorptions are stronger.

ACKNOWLEDGMENTS

One of the authors (P.D.) would like to thank the Grenoble High Magnetic Field Laboratory (GHMFL) which provided a very substantial part of the equipment, for the experimental support. Part of the equipment acquisition has been possible by the support of the European Union (SADOVEM Grant No. Science SC1*CT91-0711). He would also like to thank Jean Florentin (GHMFL) who provided mechanical pieces required by the setup. The calculation work has been supported by the SPHERS network (HPRN-CT-2000-00022), the INTAS project 03-51-3394, the UK Engineering and Physical Science Research Council and Natural Environment Research Council, and the Russian Fund for Fundamental Studies. We want to thank Bern Abel at University of Göttingen for providing the iodine cell, Danièle Romanini (LSP) for the design of the original ringdown control box, and Sergei V. Shirin (IAP), Oleg L. Polyansky (IAP), and Alain Campargue (LSP) for helpful discussions.

[1] A. Arking, Science **273**, 779 (1996).
[2] E. Mlawer, P. Brown, S. Clough, L. Harrison, J. Michalsky, P. Kiedron, and T. Shippert, Geophys. Res. Lett. **27**, 2653 (2000).
[3] L. Rothman, D. Jacquemart, A. Barbe *et al.*, J. Quant. Spectrosc. Radiat. Transf. **96**, 139 (2005).
[4] H. Partridge and D. Schwenke, J. Chem. Phys. **106**, 4618 (1997).
[5] M. Carleer, A. Jenouvrier, A.-C. Vandaele, P. Bernath, M. Mérienne, R. C. N. Zobov, O. Polyansky, J. Tennyson, and V. Savin, J. Chem. Phys. **111**, 2444 (1999).
[6] R. Schermaul, R. Learner, D. Newnham, J. Ballard, N. Zobov, D. Belmiloud, and J. Tennyson, J. Mol. Spectrosc. **208**, 32 (2001).
[7] J. Tennyson, N. Zobov, R. Williamson, O. Polyansky, and P. Bernath, J. Phys. Chem. Ref. Data **30**, 735 (2001).
[8] P. Bernath, Phys. Chem. Chem. Phys. **4**, 1501 (2002).
[9] P. Macko, D. Romanini, S. Mikhailenko, O. Naumenko, S. Kassi, A. Jenouvier, V. Tyuterev, and A. Campargue, J. Mol. Spectrosc. **227**, 90 (2004).
[10] J.-Y. Mandin, V. Dana, D. Jacquemart, N. Picqué, and G. Guelachvili, J. Quant. Spectrosc. Radiat. Transf. **78**, 353 (2003).
[11] A. Ramponi, F. Milanovich, T. Kan, and D. Deacon, Appl. Opt. **27**, 4606 (1988).
[12] M. Levenson, B. Paldus, T. Spence, C. Harb, J. S. Harris, Jr., and R. Zare, Chem. Phys. Lett. **290**, 335 (1998).
[13] B. Paldus, C. Harb, T. Spence, B. Wilke, J. Xie, J. Harris, and R. Zare, J. Appl. Phys. **83**, 3991 (1998).
[14] J. Xie, B. Paldus, E. Wahl, J. Martin, T. Owano, C. Kruger, J. Harris, and R. Zare, Chem. Phys. Lett. **284**, 387 (1998).
[15] H. Naus, W. Ubachs, P. Levelt, O. Polyansky, N. Zobov, and J. Tennyson, J. Mol. Spectrosc. **205**, 117 (2001).
[16] M. Tanaka, M. Sneep, W. Ubachs, and J. Tennyson, J. Mol. Spectrosc. **226**, 1 (2004).
[17] J. Paul, C. Collier, R. Saykally, J. Scherer, and A. O'Keefe, J. Phys. Chem. A **101**, 5211 (1997).
[18] J. Paul, R. Provençal, and R. Saykally, J. Phys. Chem. A **102**, 3279 (1998).
[19] J. Paul, R. Provençal, C. Chapo, A. Petterson, and R. Saykally, J. Chem. Phys. **109**, 10201 (1998).
[20] J. Paul, R. Provençal, C. Chapo, K. Roth, R. Casaes, and R. Saykally, J. Phys. Chem. A **103**, 2972 (1999).
[21] F. Keutsch and R. Saykally, Proc. Natl. Acad. Sci. U.S.A. **98**, 10533 (2001).
[22] C. Camy-Peyret, J.-M. Flaud, J.-Y. Mandin, J.-P. Chevillard, J. Brault, D. Ramsay, M. Vervloet, and J. Chauville, J. Mol. Spectrosc. **113**, 208 (1985).
[23] N. Zobov, D. Belmiloud, O. Polyansky, J. Tennyson, S. Shirin, M. Carleer, A. Jenouvrier, A.-C. Vandaele, P. Bernath, M. Mérienne *et al.*, J. Chem. Phys. **113**, 1546 (2000).
[24] P.-F. Coheur, S. Fally, M. Carleer, C. C. R. Colin, A. Jenouvrier, M.-F. Mérienne, C. Hermans, and A. Vandaele, J. Quant. Spectrosc. Radiat. Transf. **74**, 493 (2002).
[25] Bxl-Reims H_2O database: http://www.ulb.ac.be/cpm/datafiles.html; S. Fally (private communication).
[26] P. Theulé, Ph.D. thesis, École Polytechnique Fédérale de Lausanne, 2003.
[27] A. Callegari, P. Theulé, J. S. Muenter, R. Tolchenov, N. Zobov, O. Polyansky, J. Tennyson, and T. Rizzo, Science **297**, 993 (2002).
[28] R. Tolchenov, J. Tennyson, S. Shirin, N. Zobov, O. Polyansky, and A. Maurellis, J. Mol. Spectrosc. **221**, 99 (2003).
[29] P. Dupré, Acad. Sci., Paris, C. R. **2**, 929 (2001).

[30] *Cavity Ringdown Spectroscopy: An Ultratrace-Absorption Measurement Technique*, edited by W. Busch and M. A. Busch, Volume 720 of ACS Symposium Series, 1999.
[31] J. Scherer, P. Paul, A. O'Keefe, and R. Saykally, Chem. Rev. (Washington, D.C.) **97**, 25 (1997).
[32] M. Wheeler, S. Newman, A. Orr-Ewing, and M. Ashold, J. Chem. Soc., Faraday Trans. **94**, 337 (1998).
[33] S. Cheskis, Prog. Energy Combust. Sci. **25**, 233 (1999).
[34] A. O'Keefe, J. Scherer, J. Paul, and R. Saykally, ACS Symp. Ser. #720, edited by K. W. Busch and M. A. Busch, Washington, D.C., 1999,
[35] G. Berden, R. Peeters, and G. Meijer, Int. Rev. Phys. Chem. **19**, 565 (2000).
[36] R. Peeters, G. Berden, and G. Meijer, Am. Lab. (Shelton, Conn.) **33**, 60 (2001).
[37] D. Atkinson, Analyst (Cambridge, U.K.) **128**, 117 (2003).
[38] R. Engeln and G. Meijer, Rev. Sci. Instrum. **67**, 2708 (1996).
[39] A. O'Keefe, Chem. Phys. Lett. **293**, 331 (1998).
[40] Y. He and B. Orr, Chem. Phys. Lett. **319**, 131 (2000).
[41] R. Peeters, G. Berden, and G. Meijer, Appl. Phys. B: Lasers Opt. **73**, 65 (2001).
[42] J. Scherer, J. Paul, H. Jiao, and A. O'Keefe, Appl. Opt. **40**, 6725 (2001).
[43] A. Czyżewski, S. Chudzyński, K. Ernst *et al.*, Opt. Commun. **191**, 271 (2001).
[44] A.-C. Cheung, T. Ma, and H. Chen, Chem. Phys. Lett. **353**, 275 (2002).
[45] T. Gherman and D. Romanini, Opt. Express **10**, 1033 (2002).
[46] S. Fiedler, A. Hese, and A. Ruth, Chem. Phys. Lett. **371**, 284 (2003).
[47] A. Kastler, Nouv. Rev. Opt. **5**, 133 (1974).
[48] D. Romanini, Ann. Phys. Fr. **20**, 665 (1995).
[49] A. D. Riva, G. Zavattini, S. Marigo *et al.* Rev. Sci. Instrum. **67**, 2680 (1996).
[50] D. Romanini, A. Kachanov, and F. Stoeckel, Chem. Phys. Lett. **270**, 538 (1997).
[51] S. Brown, A. Ravishankara, and H. Stark, J. Phys. Chem. A **104**, 7044 (2000).
[52] S. Brown, H. Stark, S. Ciciora, R. McLaughlin, and A. Ravishankara, Rev. Sci. Instrum. **73**, 3291 (2002).
[53] K. Lehmann, ACS Symp. Ser. **720** 106 (1999).
[54] A. Yalin and R. Zare, Laser Phys. **12**, 1065 (2002).
[55] G. Meijer, M. Boogaarts, R. Jongma, D. Parker, and A. Wodtke, Chem. Phys. Lett. **217**, 112 (1994).
[56] K. Busch, A. Hennequin, and M. Busch, ACS Symp. Ser. **720** 33 (1999).
[57] J. Paul, L. Lapson, and J. Anderson, Appl. Opt. **40**, 4904 (2001).
[58] H. Naus, I. van Stokkum, W. Hogervorst, and W. Ubachs, Appl. Opt. **40**, 4416 (2001).
[59] D. Lee, Y. Yoon, B. Kim, J. Lee, Y. Yoo, and J. Hahn, Appl. Phys. B: Lasers Opt. **74**, 435 (2002).
[60] V. Kasyutich, C. Canosa-Mas, C. Pfrang, S. Vaughan, and R. Wayne, Appl. Phys. B: Lasers Opt. **75**, 755 (2002).
[61] D. Anderson, J. Frisch, and C. Masser, Appl. Opt. **23**, 1238 (1984).
[62] M. Lin and T. Yu, Int. J. Chem. Kinet. **25**, 875 (1993).
[63] J. Martin, B. Paldus, P. Zalicki, E. Wahl, T. Owano, J. S. Harris, Jr., C. Kruger, and R. Zare, Chem. Phys. Lett. **258**, 63 (1996).
[64] J. Poirson, F. Bretenaker, M. Vallet, and A. L. Floch, J. Opt. Soc. Am. B **14**, 2811 (1997).
[65] Y. He, M. Hippler, and M. Quack, Chem. Phys. Lett. **289**, 527 (1998).
[66] M. Hippler and M. Quack, Chem. Phys. Lett. **314**, 273 (1999).
[67] B. Paldus, C. Harb, T. Spence, R. Zare, C. Gmachl, F. Capasso, D. Sivco, J. Baillargeon, and A. Hutchinson, Opt. Lett. **25**, 666 (2000).
[68] B. Bakowski, L. Corner, G. Hancock, R. Kotchie, R. Peverall, and G. Ritchie, Appl. Phys. B: Lasers Opt. **75**, 745 (2002).
[69] A. Schocker, A. Brockhinke, K. Bultitude, and P. Ewart, Appl. Phys. B: Lasers Opt. **77**, 101 (2003).
[70] P. Birza, T. Motylewski, D. Khoroshev, A. Chirokolava, H. Linnartz, and J. Maier, Chem. Phys. **283**, 119 (2002).
[71] A. Awtry and J. Miller, Appl. Phys. B: Lasers Opt. **75**, 255 (2002).
[72] J. Hodges, J. Looney, and R. van Zee, Appl. Opt. **35**, 4112 (1996).
[73] J. Hahn, Y. Yoo, J. Lee, J. Kim, and H.-W. Lee, Appl. Opt. **38**, 1859 (1999).
[74] D. Romanini, A. K. N. Sadeghi, and F. Stoeckel, Chem. Phys. Lett. **264**, 316 (1997).
[75] M. Mürtz, B. Frech, and W. Urban, Appl. Phys. B: Lasers Opt. **68**, 243 (1999).
[76] M. Mürtz, D. Kleine, S. Stry, H. Dahnke, P. Hering, J. Lauterbach, K. Kleinermanns, W. Urban, H. Ehlers, and D. Ristau, Environ. Sci. & Pollut. Res. **4**, 61 (2002).
[77] A. Popp, F. Müller, F. Kühnemann, S. Schiller, G. von Basum, H. Dahnke, P. Hering, and M. Mürtz, Appl. Phys. B: Lasers Opt. **75**, 751 (2002).
[78] G. von Basum, D. Halmer, P. Hering, M. Mürtz, S. Schiller, F. Müller, A. Popp, and H. Dahnke, Opt. Lett. **29**, 797 (2004).
[79] W. Simpson, Rev. Sci. Instrum. **74**, 3442 (2003).
[80] M. Levenson, B. Paldus, T. Spence, C. Harb, R. Zare, M. Lawrence, and R. Byer, Opt. Lett. **25**, 920 (2000).
[81] C. Ishibashi and H. Sasada, Jpn. J. Appl. Phys., Part 1 **38**, 920 (1999).
[82] J. Ye and J. Hall, Phys. Rev. A **61**, 061802/1 (2000).
[83] Y. He and B. Orr, Chem. Phys. Lett. **335**, 215 (2001).
[84] Y. He and B. Orr, J. Chin. Chem. Soc. (Taipei) **48**, 591 (2001).
[85] Y. He and B. Orr, Appl. Phys. B: Lasers Opt. **75**, 267 (2002).
[86] J. Cachenaut, C. Man, P. Cerez, A. Brillet, F. Stoeckel, A. Jourdan, and F. Hartmann, Rev. Phys. Appl. **14**, 685 (1979).
[87] S. Gerstenkorn, J. Vergès, and J. Chevillard, *Atlas du Spectre d'Absorption de la Molècule d'Iode: 11000–14000 cm^{-1}* (Orsay, France, 1982), Vol. III.
[88] *IODINESPEC* (Toptica Photonics, Munich, Germany), www.toptica.com
[89] P. Dupré, Program MULTILINE.
[90] R. Tochenov, Program GOBLIN.
[91] O. Polyansky, A. Császár, S. Shirin, N. Zobov, P. Barletta, J. Tennyson, D. Schwenke, and P. Knowles, Science **299**, 539 (2003).
[92] O. Polyansky, N. Zobov, S. Viti, J. Tennyson, P. Bernath, and L. Wallace, Astrophys. J. **489**, L205 (1997).
[93] S. Shirin, O. Polyansky, N. Zobov, P. Barletta, and J. Tennyson, J. Chem. Phys. **118**, 2124 (2003).
[94] D. Schwenke and H. Partridge, J. Chem. Phys. **113**, 6592 (2000).
[95] N. Zobov, O. Polyansky, V. Savin, and S. Shirin, Atmos. Oceanic Optics **13**, 1024 (2000).
[96] G. Li and H. Guo, J. Mol. Spectrosc. **210**, 90 (2001).
[97] A. Callegari, P. Theulé, J. S. Muenter, R. Tolchenov, N. Zobov, O. Polyansky, J. Tennyson, and T. Rizzo (unpublished).